

# Modular Compilation for Quantum Chiplet Architectures

Mingyoung Jessica Jeng\*

mingyoungjeng@u.northwestern.edu  
Northwestern University  
Evanston, Illinois, USA

Nikola Vuk Maruszewski\*

nikola@u.northwestern.edu  
Northwestern University  
Evanston, Illinois, USA

Connor Selna

ConnorSelna2021@u.northwestern.edu  
Northwestern University  
Evanston, Illinois, USA

Michael Gavrincea

MichaelGavrincea2024@u.northwestern.edu  
Northwestern University  
Evanston, Illinois, USA

Kaitlin N. Smith

kns@northwestern.edu  
Northwestern University  
Evanston, Illinois, USA

Nikos Hardavellas

nikos@northwestern.edu  
Northwestern University  
Evanston, Illinois, USA

## ABSTRACT

As quantum computing technology continues to mature, industry is adopting modular quantum architectures to keep quantum scaling on the projected path and meet performance targets. However, the complexity of chiplet-based quantum devices, coupled with their growing size, presents an imminent scalability challenge for quantum compilation. Contemporary compilation methods are not well-suited to chiplet architectures — in particular, existing qubit allocation methods are often unable to contend with inter-chiplet links, which don’t necessary support a universal basis gate set. Furthermore, existing methods of logical-to-physical qubit placement, swap insertion (routing), unitary synthesis, and/or optimization are typically not designed for qubit links of significantly varying levels of duration or fidelity. In this work, we propose SEQC, a complete and parallelized compilation pipeline optimized for chiplet-based quantum computers, including several novel methods for qubit placement, qubit routing, and circuit optimization. SEQC attains up to a 36% increase in circuit fidelity, accompanied by execution time improvements of up to 1.92 $\times$ . Additionally, owing to its ability to parallelize compilation, SEQC achieves consistent solve time improvements of 2 – 4 $\times$  over a chiplet-aware Qiskit baseline.

## KEYWORDS

Quantum computing, quantum compilation, modular architectures.

## 1 INTRODUCTION

Classical computer systems, through the decades of their existence, have become increasingly distributed. Physical, technological, and economic constraints have prevented single “monolithic” systems from scaling to the point that they could meet the demand for high performance and yet remain practical. Today, distributed architectures are prevalent, and their latest renditions, from cloud computing to chiplet-based digital processors, are ubiquitous.

We postulate that quantum computing is on a similar path. While improvements in superconducting quantum hardware have led to the debut of processors with 1000+ qubits [13], practical implementations of quantum computation will require millions of physical qubits [34]. The number of qubits required by a quantum algorithm, the depth of the algorithm (i.e., execution time or gate count on the critical path), the auxiliary and syndrome qubits required to reach sufficiently low error rates, and the size of qubits with all control

hardware, all suggest that many more qubits are required than are likely to fit in a single die [48]. The overhead for error correction, cooling, dilution, control systems, I/O lines, challenges associated with verification and adequate chip thermalization, and realistic resources such as lossy waveguides, limited qubit fabrication yields as qubit capacity grows [44], and finite chip sizes, make the prospect of a single “monolithic” quantum processor very expensive or entirely unrealistic by current standards. These constraints force large-scale quantum systems to adopt a physically distributed architecture.

We are already observing signs of this shift. Recent developments in quantum chip linking, including flip-chip architectures [15] and low-loss coaxial cables [32], suggest that modular designs are the most viable for scaling quantum computers [44]. Many contemporary or upcoming leading quantum systems adopt chiplet-based modular quantum processors, for example using high-bandwidth quantum links between nearest-neighbor quantum chiplets (e.g., carrier-chip couplers in Rigetti Aspen-M [41, 15], or m-couplers in IBM Crossbill [14, 27]), or lower-fidelity, lower-bandwidth, but longer-distance flexible coupling of discrete chips (e.g., l-couplers in IBM Flamingo [14, 27]), or a combination of the above (e.g., c-, m-, and l-couplers in IBM Starling [27]), or multi-chip connectivity through tunable couplers and routing chips [12]. Most major companies have set their sights at modular designs to meet quantum scaling targets in practical ways, and modular quantum processors dominate their latest roadmaps [18, 17, 39].

Unfortunately, current compilation infrastructure is not capable of reasoning well about this quantum interconnect heterogeneity. The mapping of a quantum program’s logical quantum gates into the native gates supported by the underlying quantum processor, and the mapping of logical qubits to the physical qubits of the quantum hardware, largely determine the number and type of native quantum gates required for the computation, the circuit depth, and its execution time—long programs may not complete successfully as qubits decohere. Different mappings can result in vastly different compiled quantum circuits, with diverse characteristics along all these axes. These details of efficiency can make or break an algorithm in today’s noisy intermediate-scale quantum systems (NISQ) era, so quantum compilers aggressively optimize for all of them. To make matters more challenging, each qubit, coupler, and gate have diverse error profiles that are highly variable both spatially and temporally [45, 30, 8]. Unlike classical compilation that is done only once for a given architecture, quantum programs must be

\*These authors contributed equally to this work.

recompiled every time before execution, as the ideal physical qubits to execute on change between runs. So, quantum compilers today are faced with the daunting task of optimizing quantum programs across multiple dimensions with often conflicting demands, in a continuously changing environment. Coupled with the hardness of synthesizing unitaries (which is exponential in the number of qubits) and the need for quick and frequent compilation, modern quantum compilers have no option other than to rely on heuristics to perform the task. These heuristics result in a compilation complexity that we experimentally observed to be  $O(n^2)$  for  $n$  total qubits in a quantum processor, as shown in Figure 8.

Hardware modularity adds significant complexity to this already hard task, as inter-chiplet links are typically inferior compared to intra-chiplet ones [22, 44], connectivity across chiplets is often limited [14, 27], and not all basis gates are necessarily supported across chiplets [32]. In fact, popular quantum software stacks today (e.g., Qiskit [20]) are not even cognizant of the existence of hardware modularity. Hardware modularity, though, also presents an opportunity. Inspired by classical compilation, in this paper we leverage hardware modularity to achieve compilation modularity.

Compilation in classical systems is typically performed independently and in parallel for each source file, producing one object file per source. The individual object files are then linked together to construct the executable. We propose a compilation framework for modular quantum processors that works in a similar fashion: it **stratifies**, i.e., splits, the source quantum circuit into subcircuits small enough to fit in each chiplet, and maps subcircuits to chiplets, and then *in parallel* **elaborates** each subcircuit and compiles it for its target chiplet. This **Stratify-Elaborate Quantum Compiler (SEQC)** stratifies a source program only once for a given chiplet architecture, and performs only the elaboration step recurrently before each execution. In essence, SEQC replaces the recurrent  $O(n^2)$  compilation step for an  $n$ -qubit quantum processor, with several parallel  $O(k^2)$  elaboration steps for  $k$ -qubit chiplets. As the qubit capacity  $n$  of quantum processors grows exponentially, today’s  $O(n^2)$  compilation latency rises even faster. We expect, however, that the number of qubits  $k$  per chiplet will remain relatively stable or grow much slower, as it seems to be the case for the foreseeable future [18], and thus the SEQC recurrent compilation latency is expected to remain relatively stable. The stratification step is  $O(n^2)$ , so the end-to-end complexity remains the same, but stratification is performed only once; the recurrent compilation in SEQC is only  $O(k^2)$ , and barely growing with new processor designs.

Additionally, as SEQC is cognizant of hardware modularity, it can stratify the source quantum circuit into subcircuits and map them to chiplets to minimize inter-chiplet communication. As we show in this paper, SEQC produces circuits with shorter execution times and significantly fewer inter-chiplet gates compared to today’s stock compilers, leading to much higher fidelity execution. More importantly, as the number of qubits in a processor grows, SEQC achieves even higher performance in these figures of merit.

In summary, the contributions of this paper are as follows:

- We make stock compilers aware of hardware modularity, thereby allowing them to correctly compile circuits for modular architectures with limited cross-chiplet gate support.
- We design and implement SEQC, a Stratify-Elaborate Quantum Compiler for modular architectures. SEQC performs compilation in two stages, with the first stage (stratification, or chiplet splitting) performed only once for a given architecture, and the second stage (elaboration, or chiplet compilation) performed in parallel for each chiplet. Only this second stage needs to be performed before each execution, and thus SEQC’s compilation time is largely unaffected by the growth of qubit counts in future quantum processors.
- We design and implement in SEQC several novel methods for qubit placement, qubit routing, and circuit optimization.
- We evaluate SEQC and show it compiles circuits with up to 36% higher circuit fidelity and up to  $1.92\times$  lower execution time, while consistently achieving  $2-4\times$  faster compilation time compared to a chiplet-aware Qiskit baseline.

## 2 BACKGROUND AND MOTIVATION

To execute a program on a target device, the *logical* program representation must be transformed such that it conforms to the idiosyncratic *physical* constraints for that particular device. This process of logical-to-physical translation represents a critical part of compilation and is present even in exotic computing technologies, e.g., quantum. In quantum computing, programs are (usually) represented as *quantum circuits*, and devices are subject to domain-specific physical constraints, such as decoherence time [31], qubit topology (the connectivity between physical qubits) [42, 19], and the set of basis gates (the family of operations physically implemented on the device). Thus, quantum circuit *compilation* is necessary to actually run quantum programs on real-world devices.

Compilation is often divided into distinct stages such as qubit allocation (layout and routing), basis translation, and optimization. The relations between each stage and the physical constraints of both monolithic and chiplet architectures are described below.

### 2.1 Qubit Allocation

Qubit allocation addresses the topology constraints of quantum devices, where physical qubits on a device have limited connectivity to other qubits on the device. It is critical that after this stage, which often requires the modification or addition of circuit gates, the resulting optimized and technology-dependent circuit is functionally equivalent to the original, technology-independent algorithm [43]. The qubit allocation problem has been previously shown to be NP-complete [42]; thus, algorithms often adopt various strategies to make the problem more tractable. One common method is to further divide qubit allocation into two substages: *layout* and *routing*.

Logical-to-physical qubit layout, also known as qubit placement, involves deriving an injective map from the virtual qubits of the quantum circuit to the physical qubits of the quantum device [19, 23]. In other words, the qubit layout stage decides the initial position of logical qubits on the device. In contrast, qubit routing operates from an initial qubit layout and inserts SWAP operations to align a quantum circuit’s gates to a given qubit topology. Consider, for example, the state-of-the-art in qubit allocation: the SABRE heuristic search algorithm [23]. In SABRE, the distinction of the layout and

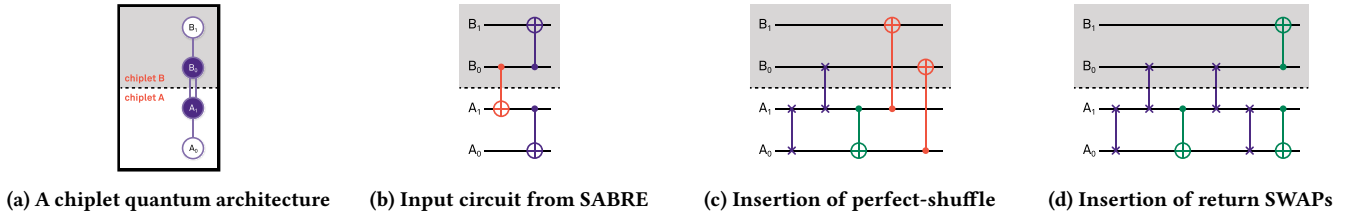


**Figure 1: Peephole correction for incompatible (non-SWAP) gates placed on inter-chiplet edges. Gates that are unimplementable on hardware are shown in red.**

routing stages motivates an iterative method for solving qubit allocation. Namely, an initial layout is used to perform qubit routing, which is used to generate a new initial layout.

Because qubit routing remains NP-hard [19], another method of simplifying the problem is to assume qubit links are roughly equivalent, particularly with respect to average fidelity and two-qubit gate duration. This assumption can manifest implicitly when a given device topology is represented as an unweighted, undirected graph. For monolithic architectures, one could debate the marginal tradeoff between performance and solution quality; however, for modular architectures, the cross-chiplet connections are far worse compared to intra-chiplet connections [44]. Thus, we could expect the solutions generated from the simplified model to be worse than a more physically accurate model, for example, in circumstances where the shortest path in terms of the quantity or depth of inserted SWAPs diverges from the shortest path in terms of fidelity, gate duration, or some combination thereof.

## 2.2 Basis Translation

Basis translation converts the gates of an input quantum circuit into gates that are physically supported on hardware. Monolithic quantum architectures typically support a so-called *universal* basis gate set, where any unitary quantum operation can be constructed using solely the gates in the set [31]. Moreover, it has been shown that basis translation can be performed efficiently given the target gate set is universal, and the quantum circuit contains a fixed, finite number of qubits [9]. Unfortunately, modular quantum architectures depend upon specialized links to connect otherwise-independent chiplets. In the general case, the cross-chiplet links can only be used for data movement (such as SWAPs) and not computation, meaning these links may not support universal operations [32]. Thus, compilers that depend on the expectation of universality among qubit links [47] and do not expect these *heterogenous, non-universal* basis gate sets can generate incompatible outputs when targeting modular architectures.

## 2.3 Optimization

Quantum circuit optimization seeks to prune extraneous operations by finding opportunities to combine, eliminate, and/or parallelize quantum gates [28]. Through commutation and cancellation identities, it is possible to search for optimization opportunities by iteratively transforming the quantum circuit without affecting the underlying operation [28]. However, in general, optimization is highly time- and resource-intensive, with the problem scaling exponentially with respect to number of qubits and/or circuit depth [21].

As a result, partitioning, the division of a quantum circuit into *blocks* of quantum gates, is a common tactic among optimization techniques [21, 49, 50]. One major consideration in this process is demarcation, i.e., where and when to draw the line between blocks. Namely, one forfeits all optimization opportunities along boundaries of demarcation, so they must be carefully chosen to minimize negative impact on the output solution. From this perspective, modular architectures are naturally synergistic with partitioning, since cross-chiplet connections present a physically motivated boundary between operations.

## 3 A STRAWMAN CHIPLET COMPILER

As discussed previously in Section 2, our model of modular quantum architectures includes the more general case where inter-chiplet links can be *non-universal*. This is representative of hardware manufacturing constraints [32], where only a restricted set of operations, e.g., state transfers or SWAPs, may be supported over long-distance couplers (inter-chiplet links). However, many compiler designs (including designs for modular architectures, see Section 7) experience errors or crashes when presented with non-universal, heterogenous, basis gate sets. For example, the Qiskit compiler [20] is explicit in its compatibility for only universal basis gate sets [47]. While it is possible to create a Qiskit Backend that supports heterogeneous basis gate sets, the compiler itself does not take them into account. Specifically, the Qiskit routing stage [52] (an implementation of SABRE) will freely place gates on incompatible physical links, and there are no methods in the compiler to prevent or fix consequent errors. For the purposes of this work, however, it was critical to establish a baseline representative of the current state of quantum compilation, against which we can compare our more-optimized design (see Section 4). Thus, we created a “Strawman” baseline compiler, built on top of the Qiskit compiler [20], with the minimal modifications necessary to generate valid outputs for chiplet architectures.

To accomplish this, we leverage a “peephole” compilation pass, which is commonly used in classical compilation to perform optimization [2]. Peephole passes operate within a nominal peephole window and substitute its contents with a logically-equivalent replacement. Notable examples in the context of quantum compilation include basis translation and elimination of self-adjoint gates. This design strategy facilitates modular compilation, not only in the sense that it can be easily parallelized, but also because peephole passes can be added between other compilation passes without breaking compatibility. These qualities make a peephole pass well-suited to the Strawman baseline, since we do not want

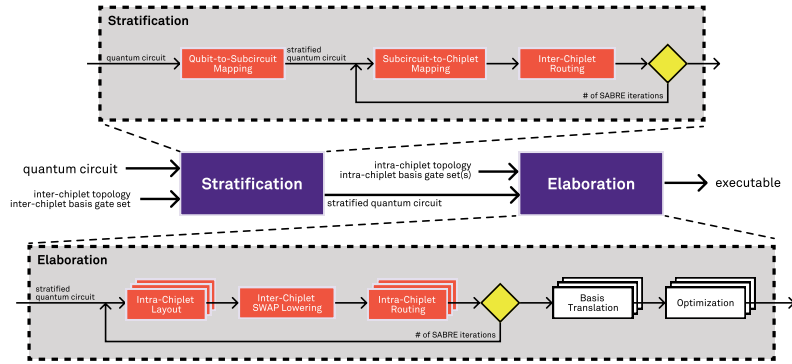


Figure 2: High-Level Diagram of SEQC. Elements in red reflect modifications from existing compiler designs.

to make extensive modifications to any of Qiskit’s built-in compilation stages or passes, nor introduce a significant performance overhead. The peephole pass used in the Strawman compiler is inserted between the routing and translation compilation stages in Qiskit. As shown in Figure 1, it operates on the circuit generated by SABRE [52], where it detects when non-SWAP gates are placed on non-universal inter-chiplet links and employs a cyclic qubit rotation, i.e., a perfect shuffle permutation, to move the aforementioned gates to nearby intra-chiplet links (see Figure 1c). Overall, for every inter-chiplet gate in the original circuit generated by SABRE, the peephole pass inserts 4 additional SWAP gates—2 inter-chiplet and 2 intra-chiplet. Ultimately, this degree of overhead is inevitable when the stock, unmodified compiler is ignorant of chiplet-specific device constraints.

To emphasize the rigor of the Strawman, it is worth discussing the designs that were ultimately discarded. For example, consider a hypothetical alternative design that skips the final peephole step shown in Figure 1d. This would appear to save 2 SWAPs, thus halving the cost per inter-chiplet gate. However, the hypothetical pass would also no longer be a true peephole, since it introduces a net qubit permutation that propagates to downstream gates in the circuit. From the perspective of modular compilation, this results in serial dependencies that prevent parallel execution of the pass. From a routing perspective, the resultant qubit permutations disrupt the solution generated by SABRE, leading to destructive routing errors that can only be resolved by an entirely new routing pass. Overall, such a hypothetical pass results in substantially worse output circuits compared to the peephole method, which we confirmed through testing. Other potential improvements on the peephole design that avoid the placement of return SWAPs would involve extensive modifications to Qiskit’s compilation stages or its underlying passes. In Section 4, we will explore such a modification of SABRE that accounts for the only-the-fly changes in qubit layout associated with inter-chiplet routing as an element of our design, in addition to numerous other components to optimize compilation for modular quantum architectures.

## 4 THE DESIGN OF SEQC

We incorporate the hierarchical elements of chiplet architectures into our compiler design by adopting a two-stage procedure, as

shown in Figure 2. The first, **stratification stage**, represents a one-time overhead to elevate a quantum circuit to the chiplet level. The second, **elaboration stage**, represents a recurring cost to complete the compilation of a quantum circuit given the most up-to-date backend properties.

### 4.1 Stratification Stage

In this stage, we map a quantum circuit to the inter-chiplet device topology, e.g., the structure in Figure 3a, by stratifying it into smaller, interconnected *subcircuits*. This can be accomplished with the following intermediate steps, as shown in Figures 3b–3d. First, **qubit-to-subcircuit mapping** designates which logical qubits belong to which logical subcircuits. Then, as part of **chiplet allocation**, we define a mapping of logical subcircuits to physical chiplets on the target device and route inter-chiplet gates to conform with constraints of physical-chiplet connectivity.

**4.1.1 Qubit-to-Subcircuit Mapping.** Qubit-to-subcircuit mapping produces a *stratified* quantum circuit, where logical qubits are grouped into subcircuits, as shown in Figure 3b. An optimal qubit-to-subcircuit mapping minimizes the number of connections between subcircuits, thereby reducing the number of inter-chiplet SWAPs needed to transfer data between chiplets during execution. To perform this task, we leverage simulated annealing, an efficient stochastic optimization technique shown to work well on NP-complete problems, such as place-and-route in VLSI algorithms [40].

Simulated annealing is an iterative method to optimize a state against a given cost function. In each iteration, the state is “kicked,” or randomly perturbed, and the new state is greedily accepted if there is a reduction in cost. However, the algorithm may randomly also accept worse solutions to escape from local minima wells. The runtime of simulated annealing is statically determined using constant tuning parameters, thus the overall complexity is determined by the complexity of the cost and kick functions, which are typically polynomial. Additionally, since each run of a simulated annealing is randomized and independent, it is possible to run multiple trials in parallel with different initial random seeds, then pick the best result. This improves the chances of finding a (near-)optimal solution.

Our method is shown in Algorithm 1. We start with an initial qubit-to-subcircuit mapping, which we minimize against a cost

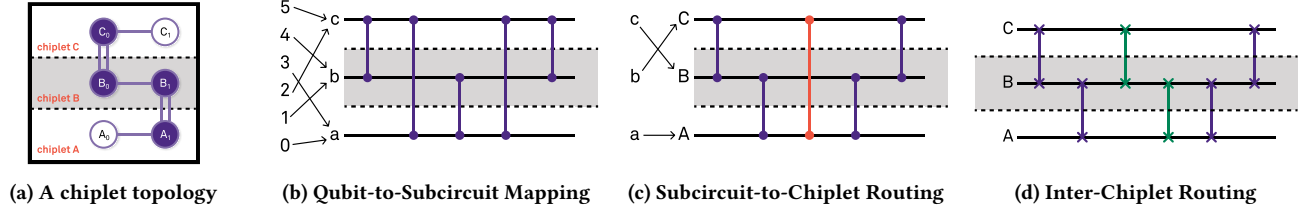


Figure 3: Step-by-step example of inter-chiplet compilation in the Stratification stage.

**Algorithm 1** Qubit-to-Subcircuit Mapping

```

1: procedure COST( $Circ, L$ )
2:    $C \leftarrow 0$  ▷ Count
3:   for  $g \in \text{TwoQubitGates}(Circ)$  do
4:      $q_0, q_1 \leftarrow \text{Qubits}(g)$ 
5:      $s_0, s_1 \leftarrow L[q_0], L[q_1]$ 
6:     Increment  $C$  if  $s_0 \neq s_1$ 
7:   return  $C$ 
8: procedure KICK( $D, N_C, N_Q, L$ )
9:    $L' \leftarrow \text{COPY}(L)$ 
10:  for  $i = 1, \dots, D$  do
11:     $s_0 \leftarrow \text{RANDCHOICE}(\{1, \dots, N_C\})$ 
12:     $q_0 \leftarrow \text{RANDCHOICE}(L'[s_0])$ 
13:     $s_1 \leftarrow \text{RANDCHOICE}(\{1, \dots, N_C\} - \{s_0\})$ 
14:     $q_1 \leftarrow \text{RANDCHOICE}(L'[s_1])$ 
15:    ▷ Swap  $q_0$  and  $q_1$  ◀
16:     $L'[s_0] \leftarrow (L'[s_0] \cup \{q_1\}) - \{q_0\}$ 
17:     $L'[s_1] \leftarrow (L'[s_1] \cup \{q_0\}) - \{q_1\}$ 
18:  return  $L'$ 
19: procedure Q2SMAPPING( $Circ, N_C, N_Q, T_0, \alpha, \beta$ )
20:   $L \leftarrow \text{Initial Layout}$  ▷ Current Solution
21:   $R \leftarrow L$  ▷ Best Solution
22:   $T \leftarrow T_0$  ▷ Annealing "Temperature"
23:  while  $T > 1$  do
24:     $D \leftarrow \text{CEIL}(T \times \alpha)$  ▷ Number of changes to make
25:     $L' \leftarrow \text{KICK}(D, N_C, N_Q, L)$ 
26:     $\Delta \leftarrow \text{COST}(Circ, L') - \text{COST}(Circ, L)$ 
27:     $k \leftarrow \text{RAND}(0, 1)$  ▷ Random number in  $[0, 1) \subset \mathbb{R}$ 
28:     $L \leftarrow L'$  if  $(\Delta < 0)$  or  $(k > \exp(\Delta/T))$ 
29:     $R \leftarrow L'$  if  $(\text{COST}(Circ, L') < \text{COST}(Circ, R))$ 
30:     $T \leftarrow T \times \beta$  ▷ Decrease temperature
31:  return  $R$ 
    
```

function, defined on line 1 as the number of inter-chiplet gates given a certain layout. By minimizing the number of inter-chiplet gates, we implicitly reduce the inter-chiplet connectivity. The kick function then swaps random qubits in the layout, ensuring that each SWAP is between qubits in different subcircuits. In doing so, we hope to move strongly interacting qubits close-together, minimizing the number of cross-chiplet gates. As input, our algorithm takes the input circuit, the chiplet count  $N_C$ , the chiplet size  $N_Q$ , the starting temperature  $T_0$ , the number of changes to do per degree of temperature  $\alpha$ , and the cooling modifier  $\beta$ . The last three are tuning parameters that do not change across runs.

**4.1.2 Chiplet Allocation.** Chiplet allocation describes the process of transforming a stratified circuit to be compatible with the inter-chiplet topology of a modular device. In Figure 2, we decompose

**Algorithm 2** Inter-Chiplet Routing

```

1: procedure FINDSWAPS( $Q, E$ )
2:   return FINDSYMBIOTICSWAPS( $Q, E$ ) if non-empty
3:   return FINDCOMMENSALISTICSWAPS( $Q, E$ ) if non-empty
4:   return FINDPARASITICSWAPS( $Q, E$ )
5: procedure VALIDGATES( $Q, L$ )
6:   Initialize  $V_{virt}$  and  $V_{phys}$  to empty sets
7:   for  $g \in Q$  do
8:      $H \leftarrow \{L[q] \mid q \in \text{Qubits}(g)\}$  ▷ Get chiplet info
9:     if  $|H| = 1$  then ▷ All qubits on same chiplet
10:      Add  $g$  to  $V_{virt}$  and  $(g, H)$  to  $V_{phys}$ 
11:   return  $V_{virt}, V_{phys}$ 
12: procedure STEP( $Q, R, L, D$ ) ▷ Advances the "wavefront"
13:    $V_{virt}, V_{phys} \leftarrow \text{VALIDGATES}(Q, L)$ 
14:    $R \leftarrow R + V_{phys}$ 
15:   for  $g \in V_{virt}$  do
16:     Remove  $g$  from  $Q$ 
17:     for  $c \in \text{CHILDREN}(g, D)$  do
18:       Add  $c$  to  $Q$  if  $p \in R$  for all  $p \in \text{PARENTS}(c, D)$ 
19: procedure HEURISTIC( $S, R, Circ$ )
20:   $L' \leftarrow \text{SWAP}(\text{COPY}(L), S)$ 
21:   $C \leftarrow 0$ 
22:  for  $g \in \text{TwoQubitGates}(Circ)$  do
23:    if  $g \notin R$  then
24:       $q_0, q_1 \leftarrow \text{Qubits}(g)$ 
25:       $s_0, s_1 \leftarrow L[q_0], L[q_1]$ 
26:      Increment  $C$  if  $s_0 \neq s_1$ 
27:  return  $C$ 
28: ▷  $L$  is from Algorithm 1,  $T$  is the chiplet topology. ◀
29: procedure INTERCHIPLETROUTING( $Circ, L, T$ )
30:   $D \leftarrow \text{CIRCUITToDAG}(Circ)$ 
31:   $E \leftarrow \text{All-pairs distances from chiplet topology } T$ 
32:   $Q \leftarrow \text{FIRSTLAYER}(DAG)$ 
33:   $R \leftarrow \text{empty list}$ 
34:  STEP( $Q, R, L, D$ )
35:  while  $Q$  is not empty do
36:     $S \leftarrow \text{FINDSWAPS}(Q, E)$  ▷ SWAP Candidates
37:     $S \leftarrow \arg \min_{s \in S} \text{HEURISTIC}(s, R, Circ)$ 
38:    SWAP( $L, S$ )
39:    STEP( $Q, R, L, D$ )
40:   $D' \leftarrow \text{Empty DAG}$ 
41:  Append  $g$  to  $D'$  for each  $g \in R$  ▷  $R$  is ordered
42:  return DAGToCIRCUIT( $D'$ )
    
```

chiplet allocation into subcircuit-to-chiplet mapping and inter-chiplet routing, analogous to how qubit allocation can be decomposed into qubit layout and routing. Accordingly, subcircuit-to-chiplet mapping, shown in Figure 3c, defines an initial placement of

logical subcircuits to physical chiplets. Subsequently, inter-chiplet routing, shown in Figure 3d, inserts inter-chiplet SWAPs to account for limited cross-chiplet gate connectivity.

In our design, we do not explicitly derive a subcircuit-to-chiplet mapping. Rather, we extend and modify the SABRE algorithm [23] to apply to chiplets, thereby using iterations of inter-chiplet routing with randomized permutations to inform a subcircuit-to-chiplet mapping. Inter-chiplet routing seeks to consolidate the qubits of (non-SWAP) inter-chiplet gates to a single chiplet by inserting inter-chiplet SWAPs into the stratified circuit. For a single two-qubit, inter-chiplet gate, we represent inter-chiplet routing as a shortest-path problem, where the two qubits of the gate correspond to chiplet endpoints in the unweighted inter-chiplet connectivity graph. From the shortest path, we can derive an optimal sequence of SWAPs for routing, where the unweighted path length, or chiplet distance, indicates the length of the SWAP chain.

However, in the context of an entire stratified circuit, composed of multiple inter-chiplet gates, it becomes possible to interleave otherwise efficiently reorder execution of SWAP chains to reduce the depth and/or total number of inter-chiplet SWAPs. Like qubit routing, we would expect it to be impractical to derive an optimal solution for this more complex picture of inter-chiplet routing at compile-time. Thus, we employ a similar SWAP selection scheme as SABRE [23], where inserted SWAPs are chosen from a pool of SWAP candidates according to a cost heuristic. For our inter-chiplet routing algorithm, we categorize SWAPs from our candidate pool into three tiers, based on a concept of the “efficiency” of each SWAP, as shown in Algorithm 2. An inter-chiplet SWAP is considered **symbiotic** if it directly affects two inter-chiplet gates in a “beneficial” manner. In other words, each qubit of a symbiotic SWAP corresponds to a different inter-chiplet gate, where the insertion of the SWAP reduces the chiplet distance score of both gates. In theory, this outcome represents the most efficient possible insertion for a single SWAP, and thus should be the highest-priority case for our greedy inter-chiplet routing cost heuristic. Next, **commensalistic** SWAPs are those that do not “harm,” or increase that chiplet distance, of any directly impacted gates. These SWAPs typically occur when an idle qubit can be used as an ancilla qubit to facilitate the routing of an inter-chiplet gate without affecting other inter-chiplet gates. In certain device topologies, a SWAP acting on the qubits of two inter-chiplet gates can also exhibit commercialistic behavior. Finally, **parasitic** SWAPs act on the qubits of two inter-chiplet gates, where one gate benefits while the other is harmed. Since this variety of SWAP is actively counterproductive towards a gate, it should be, and likely will be, avoided in most circumstances. However, given a particularly onerous circuit, it may be necessary in such rare instances to break out of a deadlock. For example, clearing one gate may free physical qubits to help route others.

## 4.2 Elaboration Stage

Following the stratification stage, each chiplet can be compiled almost completely independently from one another. More precisely, the compilation process within each chiplet is largely identical to that of a monolithic quantum architecture. The only exception is the presence of inter-chiplet SWAPs, which must be lowered from the chiplet level to the qubit level. Once this assignment is

made, these SWAPs must remain fixed and immutable to subsequent compilation stages. Despite this overhead, restricting the task of compilation to a narrower domain of qubits facilitates both parallelization (since each subcircuit can be processed in parallel) and problem size reduction (since there are fewer qubits to consider) of the most computationally intensive compilation stages, namely routing and optimization. To accomplish these tasks, we divide the elaboration stage into two substages: **qubit allocation** and **parallel basis translation and optimization**. Figure 4 illustrates this with an example of elaboration for a single chiplet in Figure 4a and its corresponding subcircuit in Figure 4b.

**4.2.1 Qubit Allocation.** Like other qubit allocation schemes, we incorporate layout (see Figure 4c) and routing (see Figure 4e) substages. However, the presence of inter-chiplet gates also necessitates several key changes to the SABRE [23] qubit allocation algorithm to achieve correctness and/or maximum parallelism.

First, the placement of inter-chiplet gates is a non-parallelizable task (due to cross-chiplet interactions) that strongly influences the layout and routing passes, which could otherwise be fully parallelized across chiplets. To account for this, we introduce a serial stage, as shown in Figure 4d, between the parallel layout and routing passes that greedily places gates on the nearest valid inter-chiplet edge. A greedy policy was chosen because inter-chiplet gates have more restrictions on valid placements compared to intra-chiplet gates, while also experiencing substantially higher error rates [44].

Once the positions of the inter-chiplet gates are settled, they must remain fixed, imposing an additional constraint on qubit routing. To promote this behavior in SABRE, we extended its cost heuristic to weigh the device topology by fidelity. This causes higher error links to assume higher costs, discouraging SABRE from moving the high-error inter-chiplet gates. As a result, SEQC achieves better solutions in the common case. However, there is nothing to prevent SABRE from incorrectly modifying any inter-chiplet SWAPs. Thus, we need to impose hard restrictions to ensure correctness. We establish two disjoint gates sets. One gate set operates strictly within a chiplet. This is the traditional gate set for a monolithic processor. The other gate set is the only one permitted to operate across chiplets, and specifically only implements inter-chiplet SWAPs. By restricting each gate set to its own disjoint part of the overall device topology, we ensure correctness across all cases.

**4.2.2 Parallel Translation and Optimization.** The remaining compilation stages of basis translation and circuit optimization can be easily parallelized at the chiplet granularity, as shown in Figure 4f. Basis translation, in particular, is embarrassingly parallel, because every gate can be translated independently from every other gate. Meanwhile, as discussed in Section 2, optimization algorithms already employ partitioning and parallelization to create tractable subproblems from intractably large circuits, facilitating a smaller problem space, lower memory usage, and faster performance. In modular quantum architectures, we physically motivate partitions through the natural chiplet boundaries, enabling us to reap the same resource and performance benefits of partitioning without compromising on solution quality.

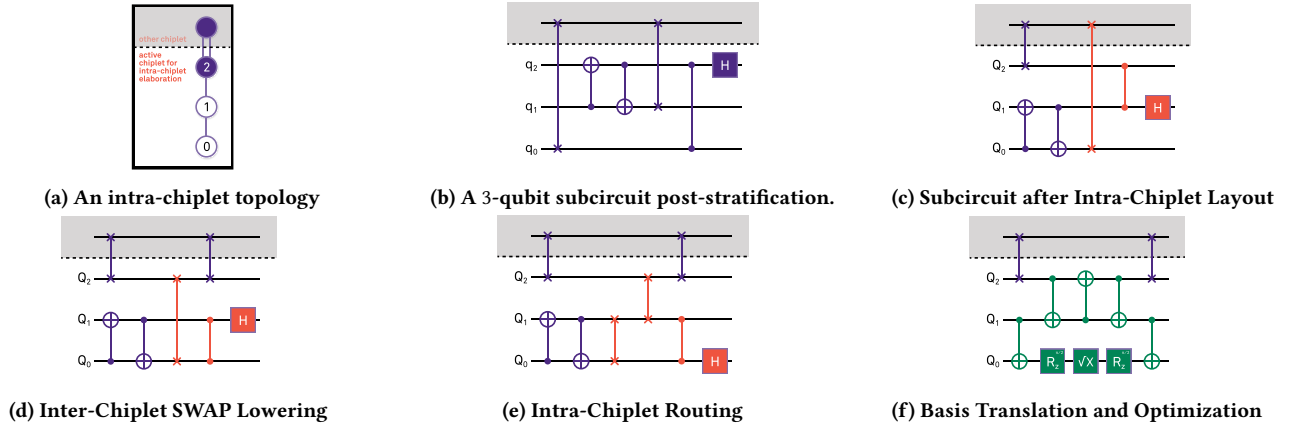


**Figure 4: Step-by-step example of intra-chiplet compilation in the Elaboration stage. Gates that cannot be implemented on hardware are shown in red.**

## 5 METHODOLOGY

To experimentally validate our compiler for modular quantum architectures, we ran a benchmark suite on a wide spectrum of circuit sizes for both SEQC and the Strawman baseline. Both SEQC and the baseline compiler were implemented in the Qiskit SDK [20] v1.2.4 and Python 3.12.6. Elaboration time results were taken on a machine with a 128-core Ampere Altra Max ARM64 processor and 256 GB of DDR4 RAM. When given a parallelizable workload, SEQC attempts to allocate its tasks evenly among the available physical cores, rounded to the nearest whole number. Finally, the simulated annealing technique used in the qubit-to-subcircuit stage uses a starting temperature  $T_0 = 200$ , a rate of change of  $0.005T$  each round,  $\frac{T}{50}$  permutations per round, and a total of 10 trials per CPU core.

### 5.1 Metrics

We compare SEQC to the Strawman baseline over a wide range of common and/or relevant metrics, discussed below. We aggregate results in a manner similar to the SPEC family of benchmarks [5], by taking the geometric mean of the relative performance ratio against a baseline technique across a benchmark suite of quantum circuits. The resultant score is then derived for each of the evaluated metrics on multiple backends of varying numbers of chiplets.

*Fidelity.* The top priority for quantum circuit execution is to maximize fidelity. Without a guarantee of correctness, the outputs of the quantum circuit are useless, and any speedup or quantum advantage is rendered moot. Fidelity is impacted by the decoherence constraints of individual qubits, as well as the errors on a gate-by-gate basis [31]. Due to simulation and hardware limitations, we utilize the estimated success probability (ESP) metric [38] to approximate fidelity. Specifically, we track the per-qubit ESP and report an aggregate ESP for each benchmark from the geometric mean of the accumulated measurements.

*Non-recurring stratification time.* This represents the time taken in the stratification stage, which will be present for our compiler and absent for the baseline. The stratification time represents a one-time overhead to prepare a quantum circuit for execution on a modular

architecture. This result can be reused for future executions on any device with an equivalent or more expansive topology.

*Recurring elaboration time.* The error characteristics of a quantum device can change on a hour-by-hour basis, or even a run-to-run basis [45, 30, 8]. Thus, to generate the highest-quality circuits with the most up-to-date characteristics possible, a given quantum circuit should be recompiled for every execution. Since the qubit and chiplet topologies remain static per-device, it is possible under the SEQC framework to reuse the results from the stratification stage, and only incur overhead from repeating the elaboration stage.

*Solve time.* This metric is relevant only to the baseline Strawman chiplet compiler, and represents the time it takes to compile a quantum circuit. The baseline compiler solve time is a recurring cost, i.e., this compilation step has to be performed every time a circuit needs to execute on a quantum machine.

*Estimated execution time.* The per-shot execution time of a quantum circuit is determined by the critical path of gate operations weighted by gate duration. In addition to performance concerns, execution time indirectly affects fidelity on NISQ-era devices due to decoherence. In other words, it is imperative that quantum circuits execute within the decoherence time to ensure high-fidelity outcomes.

*Number of inter-chiplet gates.* The inter-chiplet gates of a chiplet architecture contribute the most to error and execution time relative to other gates (at least by a factor of  $4\times$  [44]). As a result, the number of inter-chiplet gates should represent a strong proxy metric for the quality of a compiler solution. Accordingly, minimizing the number of inter-chiplet gates should result in higher fidelity, faster-executing quantum circuits.

*Circuit depth.* Defined as the unweighted critical path of a quantum circuit [31], the circuit depth is often employed as a backend-agnostic metric for execution time that can be measured statically. Notably, it is used in SABRE [23] as part of its cost heuristic.

*Gate count.* Similar to circuit depth, the total number of gates in a circuit can also be used as a static, backend-agnostic metric for certain properties of the aforementioned circuit. For instance, it may provide an indication of the amount of accumulated error, or,

like circuit depth, the execution time. SABRE [23] uses gate count to decide between randomly seeded allocation trials.

## 5.2 Benchmarks

For our benchmark suite, we leverage a subset of circuits from the Supermarq [46] suite. The circuits are chosen to be representative of practical, real-world applications for quantum computing, while also being feasible to compile for a large number of qubits. In particular, our benchmark suite comprises the following quantum circuits.

*Bit Code.* Bit codes are often used to detect and correct for bit-flip errors in quantum error correction applications. For an  $n$ -qubit benchmark,  $k = \lfloor \frac{n+1}{2} \rfloor$  data qubits are prepared in an initial state of  $|1010\dots10\rangle$  and fed through two rounds of error correction. From a compilation perspective, the structure of the bit code circuit, shown in Figure 5a, invites many opportunities for gate-level parallelism. However, because each logical qubit is connected with its two neighbors with CNOT operations, a compiler with an ill-suited topology may struggle to exploit that parallelism due to the number of necessary inserted SWAPs.

*Phase Code.* Like the bit code, phase codes are often used to detect and correct for phase-flip errors in quantum error correction applications. For an  $n$ -qubit benchmark,  $k = \lfloor \frac{n+1}{2} \rfloor$  data qubits are prepared in an initial state of  $|1010\dots10\rangle$  and fed through two rounds of error correction. To the compiler, the main difference compared to the bit code circuit is the presence of additional single-qubit gates, as shown in Figure 5b. This may showcase a compiler’s ability to do noise-aware mapping by differentiating between the relative cost (duration and/or fidelity) between a single-qubit gate and a two-qubit gate.

*Greenberger–Horne–Zeilung (GHZ).* Entanglement is one of the fundamental properties of quantum states and a major source of quantum advantage. The GHZ state represents a maximally entangled  $n$ -qubit state of  $\frac{1}{\sqrt{2}}(|0\rangle^{\otimes n} + |1\rangle^{\otimes n})$ . The algorithmic circuit structure is essentially a single chain of CNOT gates, as shown in Figure 5c. From a compilation perspective, this represents a pure exercise in qubit allocation, because the logical circuit is entirely serial. An  $n$ -qubit GHZ circuit that fully utilizes a  $k$ -chiplet device should necessitate  $\lfloor \frac{n}{k} \rfloor - 1$  logical CNOT operations to extend between chiplets. In turn, this will necessitate at least  $2 \left( \lfloor \frac{n}{k} \rfloor - 1 \right)$  inter-chiplet SWAPs to transfer qubit in and out of a chiplet.

*VQE.* The variational quantum eigensolver (VQE) [36] is another hybrid quantum-classical variational algorithm that is often used in chemistry applications. In our experiments, we choose a 2-layer ansatz whose parameters are again randomly generated, as shown in Figure 5d. This results in a quantum circuit that is essentially two CNOT chains separated by single-qubit operations. The CNOT chains can be interleaved, which in conjunction with the single-qubit gates, creates many opportunities for parallelism (resembling pipelining in classical computing). Moreover, from a qubit routing perspective, the second CNOT chain forces the compiler to consider how qubit permutations in one circuit layer propagate to future layers.

*Hamiltonian Simulation.* Quantum devices are naturally well-suited to simulating Hamiltonians. The Supermarq benchmark selects the 1D Transverse Field Ising Model (TFIM) system to model,

which is relevant for phase transitions in magnetic materials. The circuit for Hamiltonian Simulation, shown in Figure 5e, resembles a slightly more complex GHZ circuit, including how it is completely serial. Compared to GHZ, this circuit should test the compiler’s ability to lookahead during routing to detect back-to-back gates on the same two-qubit pair, while also emphasizing parallelism originating from the efficient placement of SWAP gates.

## 5.3 Simulated Quantum Device Specifications

We perform our experiments on mock backends that are generated to conform to the chiplet architecture proposed in Smith et al. [44]. The hardware specifications of the qubits and intra-chiplet connections are sourced from Acharya et al. [1]. Table 1 details the full specifications. To generate the expected fidelity of the inter-chiplet SWAPs, we perform a simulated random benchmarking trial and calculate the error rate of a SWAP gate with these backend specifications. Following Smith et al. [44], we model *inter*-chiplet SWAPs on this backend with  $4\times$  the *intra*-chiplet error rate. Similarly, we approximate the duration of the *inter*-chiplet SWAP gate as  $4\times$  the duration of an *intra*-chiplet SWAP.

T1 [1]	$20 \times 10^{-6}$ seconds
T2 [1]	$30 \times 10^{-6}$ seconds
Frequency [1]	$6 \times 10^9$ Hz

(a) Qubit Properties.

Instruction	Duration (ns)	Error
X [1]	25	0.109%
SX [1]	25	0.109%
$R_z(\phi)$ [1]	0	0.00%
CZ (intra-chiplet) [1]	34	0.605%
SWAP (inter-chiplet)	702.4	10.23%
Reset [1]	500	0.186%
Measure [1]	500	0.196%

(b) Instruction Properties.

Table 1: Specifications of Simulated Chiplet Backend.

The topology of the simulated device is composed of a grid lattice of symmetric chiplet modules, where each chiplet features a heavy-hexagon qubit topology [6], as shown in Figure 6. The intra-chiplet topology is constructed such that the heavy-hex structure is preserved for the global device topology (ignoring chiplet division). The tessellation requirements of each chiplet restrict valid chiplet sizes to multiples of 10; however, for our experiments, we limit the size of each chiplet to the minimum of 10 qubits due to hardware limitations. Finally, note that for each valid chiplet count, there may exist multiple valid chiplet topologies. In this work, we generate our backends to use the “most-square” topology for a given chiplet count. For example, a 12-chiplet machine would be generated with a grid of  $3 \times 4$  chiplets.

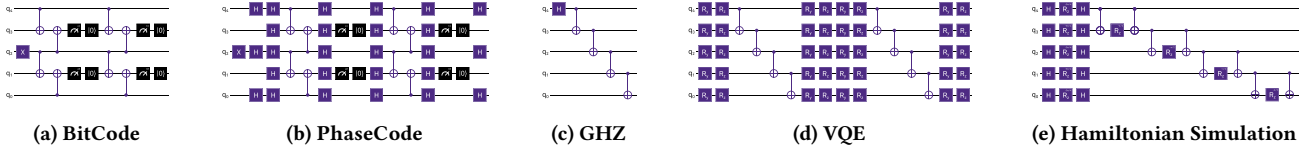


Figure 5: Examples of the Benchmark Circuits

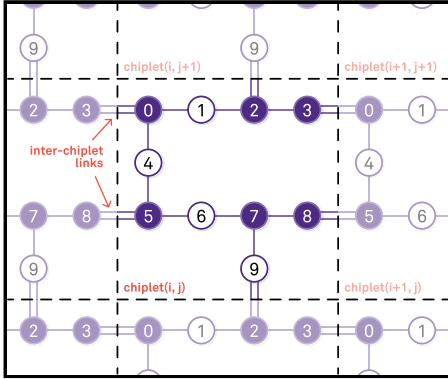


Figure 6: Construction of a grid inter-chiplet lattice from a heavy-hexagon qubit lattice, where the heavy-hex lattice is maintained for each chiplet.

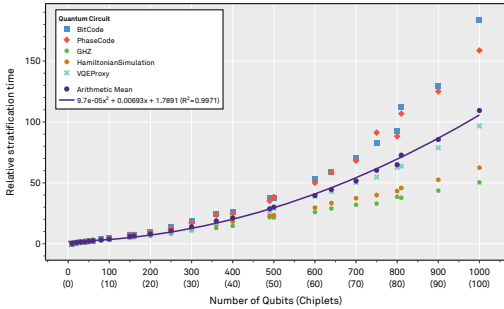


Figure 7: SEQC stratification time normalized to the 20-qubit (i.e., 2-chiplet) trial.

## 6 EXPERIMENTAL RESULTS

Figures 7–9 present measurements of the recurring compilation time (i.e., solve time) of the baseline Strawman chiplet compiler, and SEQC’s two compilation stages: the non-recurring stratification stage and the recurring elaboration stage.

The average stratification time of SEQC across the benchmark suite obeys a quadratic trajectory ( $R^2 = 0.9971$ ) with respect to the circuit size and number of chiplets, as shown in Figure 7. We note that the compilation time of the baseline, presented in Figure 8, also scales quadratically ( $R^2 = 0.9964$ ). Although stratification time represents a one-time cost, the quadratic scaling of stratification points toward the practicality of SEQC. The stratification time depends heavily on the complexity of the input circuit. Simple circuits, such as GHZ or HamiltonianSimulation, exhibit a very gradual increase

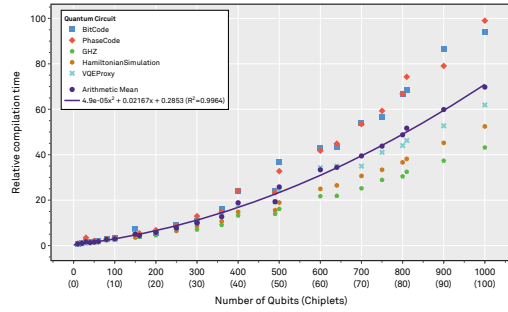


Figure 8: Baseline compilation time normalized to the 20-qubit (i.e., 2-chiplet) trial.

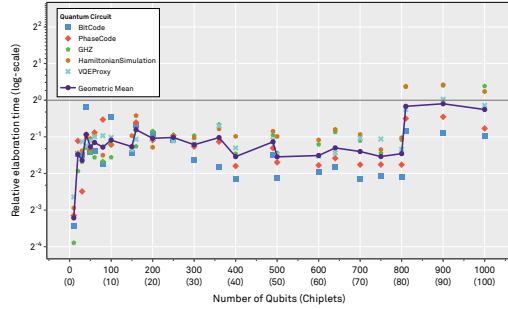
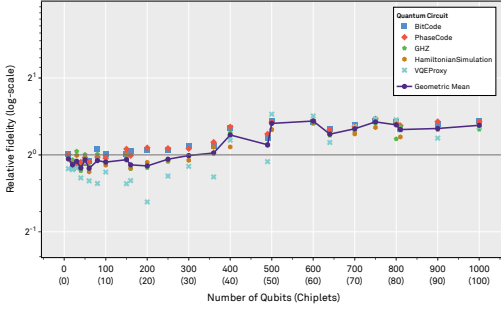


Figure 9: Relative elaboration time of SEQC normalized to the Strawman baseline for devices with 10-qubit chiplets (lower is better).

in stratification time as circuit size increases, while others, such as BitCode and PhaseCode, are much steeper. This observation holds true for the solve time of the baseline compiler as well. Collectively, these results indicate that the computational complexity of the baseline compiler and the stratification stage of SEQC are affected similarly by the same quantum circuit characteristics.

From Figure 9, we observe an improved SEQC elaboration time compared to the baseline solve time, leading to a roughly 2–4× speedup, up until 800-qubit (i.e., 80-chiplet) trials. The observed speedup reflects the expected performance improvement that our stratify-elaborate technique should garner from parallelization and problem-space reduction. For 81-chiplet experiments and above, our results begin to reflect a far more marginal speedup compared to baseline, reflecting the limitations of our evaluation hardware. Namely, as the number of chiplets begins to approach the number of physical cores and hardware threads on our hardware, SEQC experiences difficulties in evenly distributing its tasks. For example,



**Figure 10: Relative estimated fidelity (ESP) of SEQC normalized to the Strawman baseline for devices with 10-qubit chiplets (higher is better).**

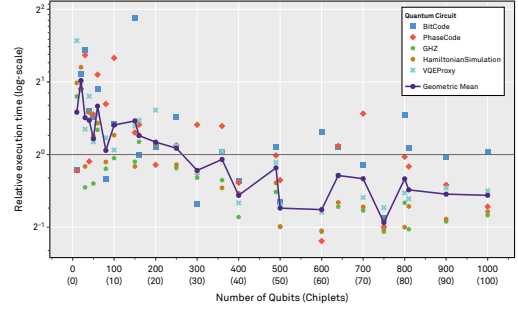
under-allocating tasks causes poor core utilization, while over-allocation leads to process thrashing, either way resulting in poorer elaboration time. However, in all cases, SEQC outperforms the baseline on average.

On a circuit-by-circuit basis, we notice higher relative performance with parallel workloads (like BitCode and PhaseCode) compared to serial workloads (GHZ and HamiltonianSimulation). Notably, above the 81-chiplet threshold where the classical machine we use for compilation no longer suffices, elaboration time exceeds the baseline solve time for the serial workloads. This is because serial circuits are fundamentally trivial to solve, and thus benefit less from the parallelism offered by SEQC. We verified experimentally that in these cases, SEQC spends almost all of its time on thread startup and teardown, rather than useful work. Moreover, the raw compilation time is trivially small in these cases, owing to the simplicity of the circuits, thus relative performance differences have little practical significance.

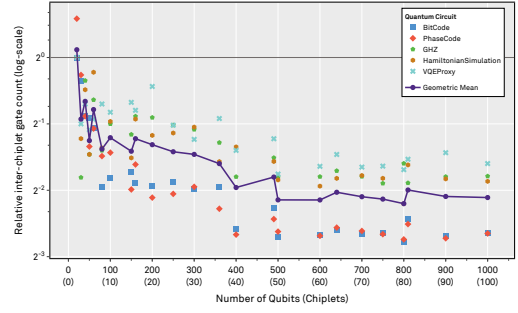
Figure 10 presents the relative estimated fidelity of SEQC compared to the baseline with respect to the number of qubits per circuit. Notably, as the number of chiplets / the circuit size increases, SEQC improves its relative fidelity against the baseline. We begin to see higher fidelity circuits in the geometric mean once the circuit size exceeds 36 chiplets, up to a maximum of 36% higher fidelity. All benchmarks reflect higher relative performance for the 50-chiplet trials and above.

Figure 11 presents the estimated per-shot execution time of the circuits produced by SEQC compared to the circuits produced by the baseline compiler, as a function of the number of qubits per circuit. As explained above, we approximate the duration of an inter-chiplet SWAP as  $4\times$  the duration of an intra-chiplet SWAP [44]. Under this model, we observe execution time benefits up to a  $1.92\times$  improvement over baseline at 750 qubits (75 chiplets). Not only are improvements in execution time desirable for quantum circuit throughput, they could also result in lower decoherence and thus improved circuit fidelity.

Figure 12 shows the number of inter-chiplet swaps in the circuits generated by SEQC relative to the circuits generated by the baseline, with respect to the number of qubits per circuit. For essentially all tested circuits, SEQC achieves a significant reduction in the number of inter-chiplet swap gates, appearing to asymptotically converge



**Figure 11: Estimated per-shot execution time of circuits produced by SEQC normalized to circuits produced by the Strawman baseline for devices with 10-qubit chiplets (lower is better).**



**Figure 12: Relative number of inter-chiplet gates for SEQC normalized to the Strawman baseline for devices with 10-qubit chiplets (lower is better).**

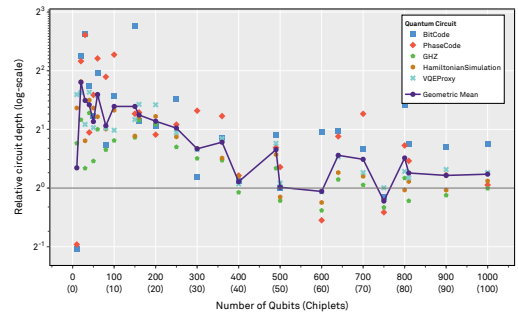


**Figure 13: Relative circuit depth of SEQC normalized to the Strawman baseline for devices with 10-qubit chiplets (lower is better).**

on a roughly  $4\times$  reduction, with the greatest reduction of  $4.6\times$  at 800 qubits / 80 chiplets. This aligns with our model of inter- vs intra-chiplet gates, where inter-chiplet SWAPs are assumed to have  $4\times$  the error [44] and  $4\times$  the gate duration.

Relative circuit depth and gate count, shown in Figures 13 and 14, respectively, share similar behavior and analysis. At small circuit

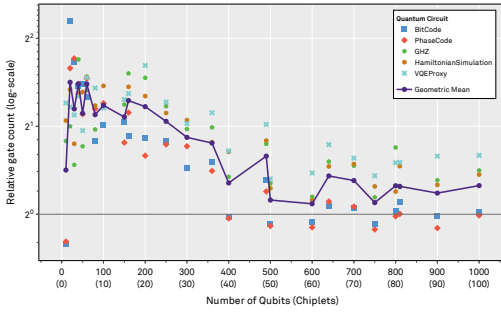


**Figure 14: Relative gate count of SEQC normalized to the Strawman baseline for devices with 10-qubit chiplets (lower is better).**

sizes, SEQC has higher circuit depth and gate count than the baseline. The gap shrinks as the circuit size increases, although SEQC always tends to perform worse on these metrics on average. This behavior is to be expected, since the baseline directly optimizes for circuit depth and gate count, while SEQC prioritizes other metrics, e.g., reducing inter-chiplet gates.

## 6.1 Discussion

The discrepancy between the circuit depth and gate count results compared to the execution time and fidelity results, respectively, are indicative of the differences between SEQC and the contemporary quantum compilers. Circuit depth and gate count represent the heuristics used in the baseline, especially SABRE [23], and they are fundamentally *unweighted* metrics. In other words, circuit depth and gate count only consider the number of gates (in the critical path and in total) irrespective of each one’s unique underlying properties. Meanwhile, SEQC is able to more directly estimate execution time and fidelity, the practically relevant metrics, by constructing *weighted* heuristics.

With the context of our static metrics (number of inter-chiplet gates, circuit depth, and gate count), it is possible to justify the improvements in relative fidelity and relative per-shot execution time as the circuit size increases. Namely, as expected, the unweighted heuristics in SABRE tend to under-represent the error and gate delay contribution of inter-chiplet gates. This effect gets exacerbated for wider or deeper circuits, which increase the number of opportunities for cross-chiplet interactions.

Overall, we observe that SEQC yields circuits with more desirable characteristics when executing on modular quantum architectures, while at the same time it achieves faster compilation times. Also, as the number of qubits increase, the performance improvement of SEQC widens compared to the baseline, especially for the most important metrics of fidelity, compiled circuit execution time, and number of inter-chiplet gates. These trends hold promise in allowing for faster and better compilation for future large-scale modular quantum devices than we can achieve with today’s frameworks.

## 7 RELATED WORK

Even though quantum computing is still nascent, there is a significant body of work on techniques for compiling quantum circuits

for NISQ processors. Here, we focus on the work that best relates to our contributions.

MECH [51] sacrifices some ancillary qubit resources to build an “adjustable multi-entry communication highway” through software. By entangling ancillary qubits and distributing them throughout the chiplet architecture’s topology, the work virtualizes those qubits into fast network-on-chip routing channels without hardware modifications. Future work to extend SEQC with MECH’s methodology may enable combining MECH’s techniques with SEQC’s allocation procedures to gain the benefits of each.

Noting the scaling challenges and fidelity issues associated with large, monolithic quantum machines, CutQC [24] establishes a hybrid computing paradigm which enables smaller-scale quantum computers to evaluate quantum circuits they would have otherwise had too few qubits to execute. To establish said paradigm, the work introduces a novel circuit-cutting technique for partitioning larger quantum circuits into small subcircuits. Classical post-processing is performed on the results of the subcircuit evaluations, merging them to find the result that would be generated by the uncut circuit. Circuit cutting as performed in CutQC served as an inspiration for SEQC’s stratification step, but unlike CutQC, SEQC does not perform any classical “stitching” of the results afterwards. It is interesting to note that our first version of SEQC was formulating the problem using constrained optimization as well, but the slowdown of the stratification step was unacceptable and impractical for large quantum circuits, and thus was abandoned in favor of the heuristics we currently employ in our compiler.

Bandic et al.[3] also note the benefits of modularity. Their study is motivated by application-specific optimization – they seek techniques that allow a quantum circuit’s structure to influence hardware architecture. They define the relationship between circuit structure and mapping efficiency, utilizing this information to optimize the architecture of single- and multi-core quantum processors.

Piveteau and Sutter [37] investigate the benefits of using *quasiprobability simulation* to allow subcircuits cut from larger quantum circuits to perform their quantum operations independently, simulating inter-chiplet link behavior where the subcircuits connect. When augmented with classical communication between circuits to reduce the simulation overhead incurred by sampling, they demonstrate that resulting circuits reach fixed accuracy with less simulation time. Unlike SEQC that targets quantum compilation, this technique has been developed to partition large quantum circuits into subcircuits that fit on smaller devices, at the cost of a simulation overhead to classically combine them.

Lin et al. [25] recognize that each 2-qubit gate in a quantum circuit has a dynamic behavioral profile which depends on manufacturing and environmental factors, and present a compilation technique which uses each 2-qubit set’s calibration data to determine potentially nonstandard 2Q gate operations which are much more ideal for that set to perform than their standard counterparts—essentially, choosing a more favorable basis. By characterizing these nonstandard gates, using their unitaries to synthesize standard gates, and essentially allowing 2Q gates to perform standard operations along bases more compatible with their respective physical states, the technique improves fidelity. This technique is orthogonal to SEQC and could work synergistically with it.

By mapping circuit partitioning to a minimum cut problem, Bandic et al. [4] use the QUBO model with quantum solvers to generate a set of cuts intended to minimize swaps between circuit partitions. QUBO employs quantum optimization algorithms on quantum annealers to accelerate the solution process and remain practical, as the search space for transmission qubits is  $2^n$ . SEQC, in contrast, does not require acceleration through quantum means, but at the cost of not guaranteeing an optimal solution (it is rather a “best-effort” approach that works well in practice).

Through discussion of scalability issues impeding the development of larger monolithic quantum circuits, Ovide et al. [33] motivate the necessity of mapping quantum circuits to multi-core architectures and present a commonly agreed-upon likely computing paradigm which leverages both quantum and classical methods to foster inter-chip communication, circumventing the scalability challenges inherent to monolithic quantum processors. While this work advocates for a two-level, hierarchical approach for quantum circuit mapping, it leaves the actual problem of qubit placement and then routing unsolved. SEQC provides an algorithm and implementation, addressing both of these challenges.

Using iterative optimization via the Hungarian algorithm, Hungarian Qubit Assignment (HQA) [10] seeks to optimize the qubit-to-core mapping problem. Because the Hungarian algorithm is here extended with the ability to adjust a qubit’s cost matrix according to behavior multiple timeslices ahead, the model can leverage lookahead to optimize further the number of inter-core swaps. However, HQA operates under the assumption that all inter-chiplet communications have the same cost, meaning chiplets must be fully connected. SEQC, on the other hand, is able to work with any arrangement of chiplets and inter-chiplet links so long there is a path between any two chiplets, taking into account the distance between pairs of chiplets to generate improved circuits.

Iterating on their previous work on Hungarian Qubit Assignment, Escofet et al. [11] develop a characterization technique for arbitrary quantum circuits which yields theoretical upper and lower optimization bounds. This is significant, since it enables optimality assessment for solutions to the qubit mapping problem.

Pastor et al. [35] leverage deep reinforcement learning to partition quantum circuits for execution across multiple processing cores. Using a DRL model enhanced with policy-masking mechanisms and a lookahead-capable observation array, the work finds valid qubit-circuit mappings for each of timeslice while prioritizing the reduction of inter-core swaps. Notably, it only considers inter-core swaps for optimization, deeming intra-core single-and-multiple qubit operations so inexpensive that their optimization should serve as fodder for inter-core swap reductions. This is sensible, but leaves optimization potential on the table, since it only seeks to generate *valid* mappings within each timeslice. Additionally, similar to HQA, this technique treats all inter-chiplet communications equally, further missing optimization opportunities with non-fully connected chiplet topologies. SEQC, in contrast, is cognizant of the differing costs of moving information between each pair of chiplets, and optimizes accordingly.

To solve the qubit allocation (mapping) problem, Liu et al. [26] develop an algorithm that combines partitioning, permutation-aware

synthesis, and a modified version of SABRE. In a bottom-up approach, this technique partitions a logical circuit into blocks, performs permutation-aware synthesis on each block in parallel (solving for all possible qubit topologies), and finally uses an augmented SABRE algorithm to perform initial layout and routing between blocks. In contrast, SEQC takes a top-down approach, where SWAP permutations between chiplets are settled prior to any compilation tasks performed within each block. As a consequence, we only need to generate solutions for one qubit layout per block, rather than synthesizing all possible block permutations.

Parallelizing SEQC’s recurrent elaboration step was inspired by traditional classical compilation techniques, which has a decades-long history and is now commonplace [29, 16]. Besides traditional compilation, though, we can also draw parallels between our work and prior research on data movement in the classical space. Data movement is widely understood to be the primary performance bottleneck in the classical architecture space. In the last two decades, work has proliferated on dataflow and spatial architectures, much of which focuses on mapping problems. Consider neural network architectures, for example, which seek to map their physical topologies as closely as possible to problem topologies. Eyeriss [7] approaches the dataflow mapping problem by proposing a row-stationary architecture, and then optimizing the mapping of problem to processing element such that elements which are spatially local in the problem are spatially local in hardware during execution. This is not unlike qubit swap optimization, and in fact is performed for many of the same reasons — like inter-chiplet swaps, data movements between more distant classical programming elements in a dataflow architecture are more expensive, and minimizing their frequency yields performance improvements.

## 8 CONCLUSION

Physical, technological and economic considerations make the prospect of a single “monolithic” large-scale quantum processor very expensive or entirely unrealistic by current standards. These constraints force future quantum systems to adopt a physically distributed architecture, based on modular quantum chiplets. As such, modular quantum processors already dominate the roadmaps of several major quantum companies.

However, the complexity of chiplet-based quantum devices, coupled with their growing size, presents an imminent scalability challenge for quantum compilation. Existing qubit allocation methods are often unable to contend with inter-chiplet links, which don’t necessarily support a universal basis gate set, and existing methods of logical-to-physical qubit placement, routing, unitary synthesis, and quantum circuit optimization, are typically not designed for qubit links that vary significantly in terms of duration or fidelity.

In this work, we first modify stock contemporary compilers to become aware of hardware modularity, thereby allowing them to correctly compile circuits for modular architectures with limited cross-chiplet gate support. We then propose SEQC, a Stratify-Elaborate Quantum Compiler for modular architectures. SEQC performs compilation in two stages, with the first stage (stratification, or chiplet splitting) performed only once for a given architecture, and the second stage (elaboration, or chiplet compilation) performed in parallel for each chiplet. Unlike contemporary quantum compilers

that have to compile a quantum circuit anew before each execution, only the elaboration stage of SEQC needs to be performed recurrently before each execution. As its computational complexity is a function of the quantum chiplet size, not the entire quantum processor size, and chiplet sizes grow slowly, SEQC's recurrent compilation time is largely unaffected by the relentless growth of qubit counts in future quantum processors.

We design and implement several novel methods for qubit placement, qubit routing, and circuit optimization in SEQC, with both hardware modularity and compilation parallelization in mind. Owing to these techniques and its parallelization strategy, SEQC compiles circuits that exhibit up to a 36% increase in circuit fidelity and up to  $1.92\times$  lower execution time, while consistently achieving 2–4 $\times$  faster compilation time over a chiplet-aware Qiskit baseline.

## ACKNOWLEDGEMENTS

This research was partially supported by NSF awards CNS-1763743 and CCF-2119069, Academic Year Undergraduate Research Award #2023-17704 by Northwestern University, and undergraduate summer research awards by the Robert R. McCormick School of Engineering and Applied Science and the Computer Science Department at Northwestern University. The authors thank Kabir Dubey for helping with earlier versions of this manuscript.

This research was supported in part through the computational resources and staff contributions provided for the Quest high performance computing facility at Northwestern University which is jointly supported by the Office of the Provost, the Office for Research, and Northwestern University Information Technology.

We acknowledge the use of IBM Quantum services for this work. The views expressed are those of the authors, and do not reflect the official policy or position of IBM or the IBM Quantum team.

## REFERENCES

- [1] Rajeev Acharya et al. 2023. Suppressing quantum errors by scaling a surface code logical qubit. *Nature*, 614, 7949, (Feb. 2023), 676–681. doi: [10.1038/s41586-022-05434-1](https://doi.org/10.1038/s41586-022-05434-1).
- [2] Alfred V. Aho, Monica S. Lam, Ravi Sethi, and Jeffrey D. Ullman. 2006. *Compilers: Principles, Techniques, and Tools (2nd Edition)*. Addison-Wesley Longman Publishing Co., Inc., USA. ISBN: 0321486811.
- [3] Medina Bandic, Pablo le Henaff, Anabel Ovide, Pau Escofet, Sahar Ben Rached, Santiago Rodrigo, Hans van Someren, Sergi Abadal, Eduard Alarcón, Carmen G. Almudever, et al. [n. d.] Profiling quantum circuits for their efficient execution on single- and multi-core architectures. *Quantum Science and Technology*.
- [4] Medina Bandic, Luise Prielinger, Jonas Nüßlein, Anabel Ovide, Santiago Rodrigo, Sergi Abadal, Hans van Someren, Gayane Vardoyan, Eduard Alarcón, Carmen G Almudever, et al. 2023. Mapping quantum circuits to modular architectures with QUBO. In *2023 IEEE International Conference on Quantum Computing and Engineering (QCE)*. Vol. 1. IEEE, 790–801.
- [5] James Bucek, Klaus-Dieter Lange, and J akim v. Kistowski. 2018. Spec cpu2017: next-generation compute benchmark. In *Companion of the 2018 ACM/SPEC International Conference on Performance Engineering (ICPE '18)*. Association for Computing Machinery, Berlin, Germany, 41–42. ISBN: 9781450356299. doi: [10.1145/3185768.3185771](https://doi.org/10.1145/3185768.3185771).
- [6] Christopher Chamberland, Guanyu Zhu, Theodore J. Yoder, Jared B. Hertzberg, and Andrew W. Cross. 2020. Topological and subsystem codes on low-degree graphs with flag qubits. *Phys. Rev. X*, 10, (Jan. 2020), 011022, 1, (Jan. 2020). doi: [10.1103/PhysRevX.10.011022](https://doi.org/10.1103/PhysRevX.10.011022).
- [7] Yu-Hsin Chen, Joel Emer, and Vivienne Sze. 2016. Eyeriss: a spatial architecture for energy-efficient dataflow for convolutional neural networks. In *Proceedings of the 43rd International Symposium on Computer Architecture (ISCA '16)*. IEEE Press, Seoul, Republic of Korea, 367–379. ISBN: 9781467389471. doi: [10.1109/ISCA.2016.40](https://doi.org/10.1109/ISCA.2016.40).
- [8] Samudra Dasgupta and Travis S Humble. 2021. Stability of noisy quantum computing devices. *arXiv preprint arXiv:2105.09472*.
- [9] Christopher M. Dawson and Michael A. Nielsen. 2006. The Solovay-Kitaev algorithm. *Quantum Info. Comput.*, 6, 1, (Jan. 2006), 81–95.
- [10] Pau Escofet, Anabel Ovide, Carmen G Almudever, Eduard Alarc on, and Sergi Abadal. 2023. Hungarian qubit assignment for optimized mapping of quantum circuits on multi-core architectures. *IEEE Computer Architecture Letters*.
- [11] Pau Escofet, Anabel Ovide, Medina Bandic, Luise Prielinger, Hans van Someren, Sebastian Feld, Eduard Alarc on, Sergi Abadal, and Carmen G. Almud ever. 2024. Revisiting the mapping of quantum circuits: entering the multi-core era. (2024). arXiv: [2403.17205](https://arxiv.org/abs/2403.17205) [quant-ph].
- [12] Mark Field, Angela Q. Chen, Ben Scharmann, Eyob A. Sete, Feyza Oruc, Kim Vu, Valentin Kosenko, Joshua Y. Mutus, Stefano Poletto, and Andrew Bestwick. 2024. Modular superconducting-qubit architecture with a multiplex tunable coupler. *Phys. Rev. Appl.*, 21, (May 2024), 054063, 5, (May 2024). doi: [10.1103/PhysRevApplied.21.054063](https://doi.org/10.1103/PhysRevApplied.21.054063).
- [13] Jay Gambetta. 2023. The hardware and software for the era of quantum utility is here. [Accessed 04-14-2024]. IBM, (Dec. 2023). <https://www.ibm.com/quantum/blog/quantum-roadmap-2033>.
- [14] Jay Gambetta and Ryan Mandelbaum. 2024. IBM quantum delivers on performance challenge made two years ago. IBM Quantum Developer Conference (<https://www.ibm.com/quantum/blog/qdc-2024>). (2024).
- [15] Alysso Gold, JP Paquette, Anna Stockklauser, Matthew J Reagor, M Sohaib Alam, Andrew Bestwick, Nicolas Didier, Ani Nersisyan, Feyza Oruc, Armin Razavi, et al. 2021. Entanglement across separate silicon dies in a modular superconducting qubit device. *npj Quantum Information*, 7, 1, 142.
- [16] T. Gross, A. Sobel, and M. Zolg. 1989. Parallel compilation for a parallel machine. In *Proceedings of the ACM SIGPLAN 1989 Conference on Programming Language Design and Implementation (PLDI '89)*. Association for Computing Machinery, Portland, Oregon, USA, 91–100. ISBN: 089791306X. doi: [10.1145/73141.74826](https://doi.org/10.1145/73141.74826).
- [17] HPCWire. 2024. IonQ plots path to commercial (quantum) advantage. Available online at: <https://www.hpcwire.com/2024/07/02/ionq-plots-path-to-commercial-quantum-advantage/>. (July 2024).
- [18] IBM. 2023. IBM debuts next-generation quantum processor & IBM quantum system two, extends roadmap to advance era of quantum utility. Available online at: <https://newsroom.ibm.com/2023-12-04-IBM-Debuts-Next-Generation-Quantum-Processor-IBM-Quantum-System-Two,-Extends-Roadmap-to-Advance-Era-of-Quantum-Utility>. (Dec. 2023).
- [19] Takehiro Ito, Naonori Kakimura, Naoyuki Kamiyama, Yusuke Kobayashi, and Yoshio Okamoto. 2023. Algorithmic theory of qubit routing. In *Algorithms and Data Structures*. Pat Morin and Subhash Suri, (Eds.) Springer Nature Switzerland, Cham, 533–546. ISBN: 978-3-031-38906-1.
- [20] Ali Javadi-Abhari, Matthew Treinish, Kevin Krsulich, Christopher J. Wood, Jake Lishman, Julien Gacon, Simon Martiel, Paul D. Nation, Lev S. Bishop, Andrew W. Cross, Blake R. Johnson, and Jay M. Gambetta. 2024. Quantum computing with Qiskit. (2024). arXiv: [2405.08810](https://arxiv.org/abs/2405.08810) [quant-ph]. doi: [10.48550/arXiv.2405.08810](https://doi.org/10.48550/arXiv.2405.08810).
- [21] Alon Kukliansky, Ed Younis, Lukasz Cincio, and Costin Iancu. 2023. Qfactor: a domain-specific optimizer for quantum circuit instantiation. In *2023 IEEE International Conference on Quantum Computing and Engineering (QCE)*. Vol. 01, 814–824. doi: [10.1109/QCE57702.2023.00096](https://doi.org/10.1109/QCE57702.2023.00096).
- [22] Nicholas LaRacuente, Kaitlin N Smith, Poolad Imany, Kevin L Silverman, and Frederic T Chong. 2022. Modeling short-range microwave networks to scale superconducting quantum computation. *arXiv preprint arXiv:2201.08825*.
- [23] Gushu Li, Yufei Ding, and Yuan Xie. 2019. Tackling the qubit mapping problem for NISQ-era quantum devices. In *Proceedings of the Twenty-Fourth International Conference on Architectural Support for Programming Languages and Operating Systems (ASPLOS '19)*. Association for Computing Machinery, Providence, RI, USA, 1001–1014. ISBN: 9781450362405. doi: [10.1145/3297858.3304023](https://doi.org/10.1145/3297858.3304023).
- [24] Gushu Li, Yufei Ding, and Yuan Xie. 2019. Tackling the qubit mapping problem for nisq-era quantum devices. In *Proceedings of the Twenty-Fourth International Conference on Architectural Support for Programming Languages and Operating Systems (ASPLOS '19)*. Association for Computing Machinery, Providence, RI, USA, 1001–1014. ISBN: 9781450362405. doi: [10.1145/3297858.3304023](https://doi.org/10.1145/3297858.3304023).
- [25] Sophia Fuhui Lin, Sara Sussman, Casey Duckering, Pranav S. Mundada, Jonathan M. Baker, Rohan S. Kumar, Andrew A. Houck, and Frederic T. Chong. 2023. Let each quantum bit choose its basis gates. In *Proceedings of the 55th Annual IEEE/ACM International Symposium on Microarchitecture (MICRO '22)*. IEEE Press, Chicago, Illinois, USA, 1042–1058. ISBN: 9781665462723. doi: [10.1109/MICRO56248.2022.00075](https://doi.org/10.1109/MICRO56248.2022.00075).
- [26] Ji Liu, Ed Younis, Mathias Weiden, Paul Hovland, John Kubiatowicz, and Costin Iancu. 2023. Tackling the qubit mapping problem with permutation-aware synthesis. In *2023 IEEE International Conference on Quantum Computing and Engineering (QCE)*. Vol. 01, 745–756. doi: [10.1109/QCE57702.2023.00090](https://doi.org/10.1109/QCE57702.2023.00090).
- [27] Ryan Mandelbaum, Antonio D. C orcoles, and Jay Gambetta. 2024. Ibm's big bet on the quantum-centric supercomputer: recent advances point the way to useful classical-quantum hybrids. *IEEE Spectrum*, 61, 9, 24–33. doi: [10.1109/MSPEC.2024.10669253](https://doi.org/10.1109/MSPEC.2024.10669253).
- [28] Dmitri Maslov, Gerhard W. Dueck, D. Michael Miller, and Camille Negrevergne. 2008. Quantum circuit simplification and level compaction. *IEEE Transactions*

- on *Computer-Aided Design of Integrated Circuits and Systems*, 27, 3, 436–444. doi: [10.1109/TCAD.2007.9113334](https://doi.org/10.1109/TCAD.2007.9113334).
- [29] M. Dennis Mickunas and Richard M. Schell. 1978. Parallel compilation in a multiprocessor environment (extended abstract). In *Proceedings of the 1978 Annual Conference (ACM '78)*. Association for Computing Machinery, Washington, D.C., USA, 241–246. ISBN: 0897910001. doi: [10.1145/800127.804105](https://doi.org/10.1145/800127.804105).
- [30] Prakash Murali, Jonathan M. Baker, Ali Javadi-Abhari, Frederic T. Chong, and Margaret Martonosi. 2019. Noise-adaptive compiler mappings for noisy intermediate-scale quantum computers. In *Proceedings of the Twenty-Fourth International Conference on Architectural Support for Programming Languages and Operating Systems (ASPLOS '19)*. Association for Computing Machinery, Providence, RI, USA, 1015–1029. ISBN: 9781450362405. doi: [10.1145/3297858.3304075](https://doi.org/10.1145/3297858.3304075).
- [31] Michael A. Nielsen and Isaac L. Chuang. 2010. *Quantum Computation and Quantum Information: 10th Anniversary Edition*. Cambridge University Press. doi: <https://doi.org/10.1017/CBO9780511976667>.
- [32] Jingjing Niu, Libo Zhang, Yang Liu, Jiawei Qiu, Wenhui Huang, Jiayang Huang, Hao Jia, Jiawei Liu, Ziyu Tao, Weiwei Wei, et al. 2023. Low-loss interconnects for modular superconducting quantum processors. *Nature Electronics*, 6, 3, 235–241.
- [33] Anabel Ovide, Santiago Rodrigo, Medina Bandic, Hans Van Someren, Sebastian Feld, Sergi Abadal, Eduard Alarcon, and Carmen G Almudever. 2023. Mapping quantum algorithms to multi-core quantum computing architectures. In *2023 IEEE International Symposium on Circuits and Systems (ISCAS)*. IEEE, 1–5.
- [34] Alexandru Paler, Daniel Herr, and Simon J Devitt. 2019. Really small shoe boxes: on realistic quantum resource estimation. *Computer*, 52, 6, 27–37.
- [35] Arnau Pastor, Pau Escofet, Sahar Ben Rached, Eduard Alarcón, Pere Barlet-Ros, and Sergi Abadal. 2024. Circuit partitioning for multi-core quantum architectures with deep reinforcement learning. *arXiv preprint arXiv:2401.17976*.
- [36] Alberto Peruzzo, Jarrod McClean, Peter Shadbolt, Man-Hong Yung, Xiao-Qi Zhou, Peter J. Love, Alán Aspuru-Guzik, and Jeremy L. O'Brien. 2014. A variational eigenvalue solver on a photonic quantum processor. *Nature Communications*, 5, 1, (July 2014), 4213. doi: [10.1038/ncomms5213](https://doi.org/10.1038/ncomms5213).
- [37] Christophe Piveteau and David Sutter. 2024. Circuit knitting with classical communication. *IEEE Transactions on Information Theory*, 70, 4, 2734–2745. doi: [10.1109/TIT.2023.3310797](https://doi.org/10.1109/TIT.2023.3310797).
- [38] Fang Qi, Kaitlin N. Smith, Travis LeCompte, Nian-feng Tzeng, Xu Yuan, Frederic T. Chong, and Lu Peng. 2024. Quantum Vulnerability Analysis to Guide Robust Quantum Computing System Design. *IEEE Transactions on Quantum Engineering*, 5, 01, (Jan. 2024), 1–11. doi: [10.1109/TQE.2023.3343625](https://doi.org/10.1109/TQE.2023.3343625).
- [39] Rigetti. 2024. Investor presentation. Available online at: <https://investors.rigetti.com/static-files/fbac3801-223f-4f0f-a207-47d25084a1d7>. (Nov. 2024).
- [40] R.A. Rutenbar. 1989. Simulated annealing algorithms: an overview. *IEEE Circuits and Devices Magazine*, 5, 1, 19–26. doi: [10.1109/101.17235](https://doi.org/10.1109/101.17235).
- [41] SiliconAngle. 2021. Rigetti debuts multichip quantum processor with 80 qubits. Available online at: <https://siliconangle.com/2021/06/29/rigetti-looks-scale-quantum-computing-modular-processor-architecture/>. (June 2021).
- [42] Marcos Yukio Siraichi, Vinicius Fernandes dos Santos, Caroline Collange, and Fernando Magno Quintao Pereira. 2018. Qubit allocation. In *Proceedings of the 2018 International Symposium on Code Generation and Optimization (CGO 2018)*. Association for Computing Machinery, Vienna, Austria, 113–125. ISBN: 9781450356176. doi: [10.1145/3168822](https://doi.org/10.1145/3168822).
- [43] Kaitlin N Smith and Mitchell A Thornton. 2019. A quantum computational compiler and design tool for technology-specific targets. In *Proceedings of the 46th International Symposium on Computer Architecture*, 579–588.
- [44] Kaitlin N. Smith, Gokul Subramanian Ravi, Jonathan M. Baker, and Frederic T. Chong. 2022. Scaling superconducting quantum computers with chiplet architectures. In *2022 55th IEEE/ACM International Symposium on Microarchitecture (MICRO)*, 1092–1109. doi: [10.1109/MICRO56248.2022.00078](https://doi.org/10.1109/MICRO56248.2022.00078).
- [45] Swamit S. Tannu and Moinuddin K. Qureshi. 2019. Not all qubits are created equal: a case for variability-aware policies for nisq-era quantum computers. In *Proceedings of the Twenty-Fourth International Conference on Architectural Support for Programming Languages and Operating Systems (ASPLOS '19)*. Association for Computing Machinery, Providence, RI, USA, 987–999. ISBN: 9781450362405. doi: [10.1145/3297858.3304007](https://doi.org/10.1145/3297858.3304007).
- [46] T. Tomesh, P. Gokhale, V. Omole, G. Ravi, K. N. Smith, J. Viszlai, X. Wu, N. Hardavellas, M. R. Martonosi, and F. T. Chong. 2022. Supermarq: a scalable quantum benchmark suite. In *2022 IEEE International Symposium on High-Performance Computer Architecture (HPCA)*. IEEE Computer Society, Los Alamitos, CA, USA, (Apr. 2022), 587–603. doi: [10.1109/HPCA53966.2022.00050](https://doi.org/10.1109/HPCA53966.2022.00050).
- [47] [n. d.] Translation Errors | IBM Quantum Documentation — docs.quantum.ibm.com. [Accessed 2025-02-20]. <https://docs.quantum.ibm.com/api/qiskit/qiskit.transpiler.passes.BasisTranslator#translation-errors%7D>.
- [48] Rodney Van Meter, Thaddeus D. Ladd, Austin G. Fowler, and Yoshihisa Yamamoto. 2010. Distributed quantum computation architecture using semiconductor nanophotonics. *International Journal of Quantum Information*, 08, 01n02, 295–323. eprint: <https://doi.org/10.1142/S0219749910006435>. doi: [10.1142/S0219749910006435](https://doi.org/10.1142/S0219749910006435).
- [49] Xin-Chuan Wu, Marc Grau Davis, Frederic T. Chong, and Costin Iancu. 2021. Reoptimization of quantum circuits via hierarchical synthesis. In *2021 International Conference on Rebooting Computing (ICRC)*, 35–46. doi: [10.1109/ICRC53822.2021.00016](https://doi.org/10.1109/ICRC53822.2021.00016).
- [50] Ed Younis, Costin C Iancu, Wim Lavrijsen, Marc Davis, Ethan Smith, and USDOE. 2021. Berkeley quantum synthesis toolkit (bqskit) v1. (Apr. 2021). doi: [10.11578/dc.20210603.2](https://doi.org/10.11578/dc.20210603.2).
- [51] Hezi Zhang, Keyi Yin, Anbang Wu, Hassan Shapourian, Alireza Shabani, and Yufei Ding. 2024. Mech: multi-entry communication highway for superconducting quantum chiplets. (2024). arXiv: 2305.05149 [quant-ph].
- [52] Henry Zou, Matthew Treinish, Kevin Hartman, Alexander Ivrii, and Jake Lishman. 2024. Lightsabre: a lightweight and enhanced sabre algorithm. (2024). <https://arxiv.org/abs/2409.08368> arXiv: 2409.08368 [quant-ph].